SOX9 promotes stress-responsive transcription of VGF nerve growth factor inducible gene in renal tubular epithelial cells

Received for publication, July 5, 2020, and in revised form, August 28, 2020 Published, Papers in Press, September 4, 2020, DOI 10.1074/jbc.RA120.015110

Ji Young Kim[1,*], Yuntao Bai[1], Laura A. Jayne[1], Ferdos Abdulkader[1], Megha Gandhi[1], Tayla Perreau[2], Samir V. Parikh[3], David S. Gardner[4], Alan J. Davidson[2], Veronika Sander[2], Min-Ae Song[5], Amandeep Bajwa[6], and Navjot Singh Pabla[1,*]

From the [1]Division of Pharmaceutics and Pharmacology, College of Pharmacy and Comprehensive Cancer Center, The Ohio State University, Columbus, Ohio, USA, the [2]Department of Molecular Medicine and Pathology, University of Auckland, Auckland, New Zealand, [3]Wexner Medical Center, The Ohio State University, Columbus, Ohio, USA, the [4]School of Veterinary Medicine and Science, University of Nottingham, Loughborough, Leicestershire, United Kingdom, the [5]Division of Environmental Health Science, College of Public Health and Comprehensive Cancer Center, The Ohio State University, Columbus, Ohio, USA, and the [6]Transplant Research Institute, James D. Eason Transplant Institute, Department of Surgery, College of Medicine, The University of Tennessee Health Science Center, Memphis, Tennessee, USA

Edited by Eric R. Fearon

Acute kidney injury (AKI) is a common clinical condition associated with diverse etiologies and abrupt loss of renal function. In patients with sepsis, rhabdomyolysis, cancer, and cardiovascular disorders, the underlying disease or associated therapeutic interventions can cause hypoxia, cytotoxicity, and inflammatory insults to renal tubular epithelial cells (RTECs), resulting in the onset of AKI. To uncover stress-responsive disease-modifying genes, here we have carried out renal transcriptome profiling in three distinct murine models of AKI. We find that *Vgf* nerve growth factor inducible gene up-regulation is a common transcriptional stress response in RTECs to ischemia-, cisplatin-, and rhabdomyolysis-associated renal injury. The *Vgf* gene encodes a secretory peptide precursor protein that has critical neuroendocrine functions; however, its role in the kidneys remains unknown. Our functional studies show that RTEC-specific *Vgf* gene ablation exacerbates ischemia-, cisplatin-, and rhabdomyolysis-associated AKI *in vivo* and cisplatin-induced RTEC cell death *in vitro*. Importantly, aggravation of cisplatin-induced renal injury caused by *Vgf* gene ablation is partly reversed by TLQP-21, a Vgf-derived peptide. Finally, *in vitro* and *in vivo* mechanistic studies showed that injury-induced *Vgf* up-regulation in RTECs is driven by the transcriptional regulator Sox9. These findings reveal a crucial downstream target of the Sox9-directed transcriptional program and identify *Vgf* as a stress-responsive protective gene in kidney tubular epithelial cells.

Acute kidney injury (AKI) is a heterogeneous clinical syndrome that is associated with adverse short- and long-term sequelae (1). AKI usually occurs in the setting of other diseases, such as sepsis (2), rhabdomyolysis (3), and cardiovascular (4) and oncological diseases (5), where the underlying disease and/or associated therapy cause abrupt loss of renal function. As a result, the pathophysiology of AKI is generally complex because of the existence of multiple etiologies such as the presence of sepsis, ischemia, and therapy-induced nephrotoxicity (6). AKI-associated mortality depends on the severity and can be significantly high in critically ill patients (7). Importantly, patients who survive an episode of AKI are at increased risk for major adverse cardiovascular events and progression to chronic kidney disease (8).

Disorders such as sepsis, cancer, and rhabdomyolysis and therapeutic interventions such as cardiac surgery and chemotherapy are associated with inflammatory, toxic, and hypoxic insults to renal tubular epithelial cells (RTECs). The resulting RTEC dysfunction and cell death are the hallmarks of AKI (9). RTEC dysfunction and renal impairment clinically manifest as systemic electrolyte and fluid imbalances, along with accumulation of metabolic waste, which can trigger multi-organ failure (7). The pathogenesis of AKI is multifaceted because of the involvement of various intracellular pathways (6, 10–12) in RTEC dysfunction and cell death (9) and the contribution of vascular (13–15) and immune cells (16, 17) in renal impairment.

Both the etiology and pathophysiology of AKI are complex. To identify common stress-responsive genes, we have carried out genome-wide transcriptome analysis in three mouse models of AKI. Our studies identify the nerve growth factor–inducible gene *Vgf* (nonacronymic; unrelated to VEGF) as a stress-responsive gene that is up-regulated during ischemic, nephrotoxic, and rhabdomyolysis-associated kidney injury. *Vgf* was originally identified as a nerve growth factor–inducible gene in a neuroendocrine cell line and is expressed in specific neurons and endocrine cells in the brain and the periphery (18). *Vgf* gene encodes a precursor polypeptide that is proteolytically cleaved to generate several bioactive peptides, the best studied of which are TLQP-21, TLQP-62, and AQEE-30 (19). In the central nervous system, the secreted Vgf-derived peptides regulate neuronal activity, survival, and progenitor proliferation (20–22). Furthermore, germline *Vgf* knockout mice have significantly reduced body weight and increased energy expenditure and are resistant to diet-induced obesity, indicating that Vgf-derived peptides are critical regulators of energy homeostasis (20, 23).

This article contains supporting information.

* For correspondence: Ji Young Kim, kim.6494@osu.edu; Navjot Singh Pabla, pabla.2@osu.edu.

© 2020 Kim et al. Published under exclusive license by The American Society for Biochemistry and Molecular Biology, Inc.

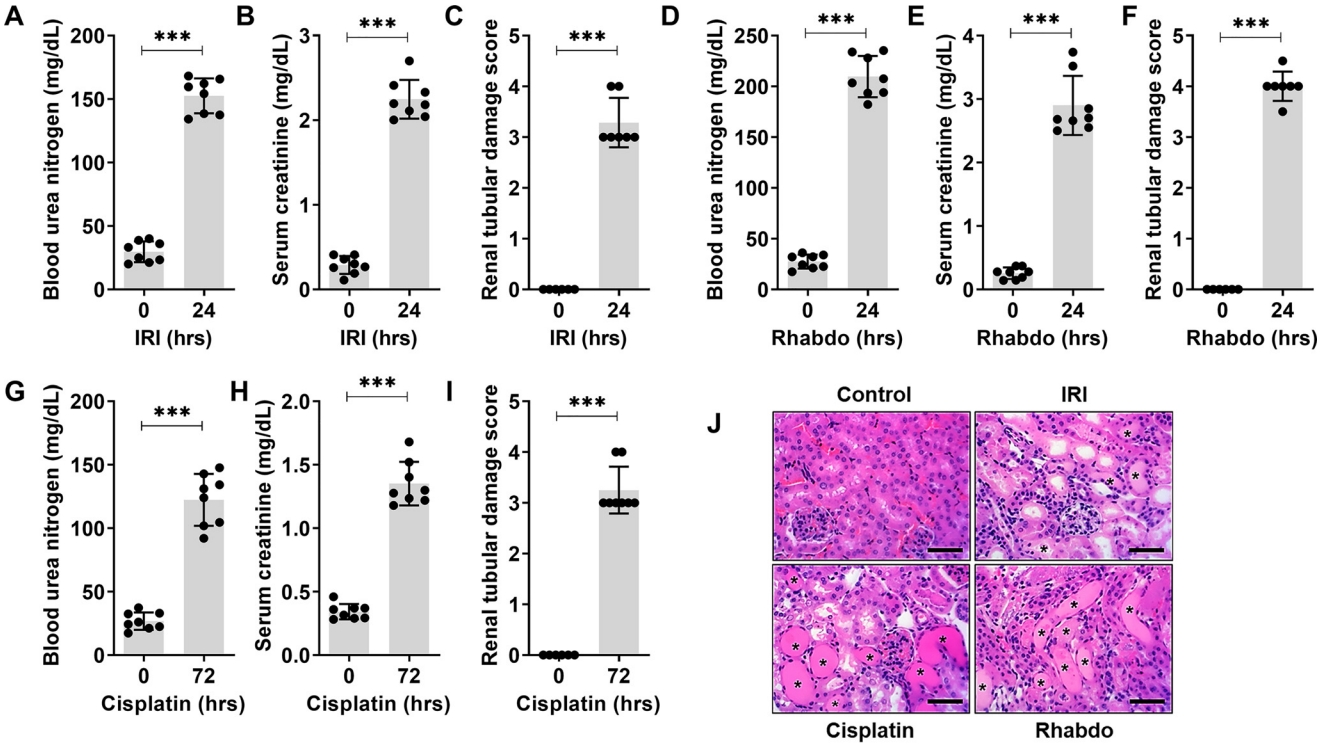

Figure 1. Mouse models of acute kidney injury. Ischemic, nephrotoxic, and rhabdomyolysis-associated acute kidney injury was induced in 8–12-week-old male C57BL/6J mice. Bilateral renal ischemia was induced for 30 min followed by reperfusion for 24 hrs. Blood urea nitrogen (*A*), serum creatinine (*B*), and histological analysis (*C*) were performed to examine renal function and damage. Rhabdomyolysis was induced in male mice by glycerol injection (7.5 ml/kg 50% glycerol) in the hind-leg muscles followed by measurement of renal function (*D* and *E*) and histological analysis (*F*) of renal damage. Nephrotoxicity was induced in mice by a single intraperitoneal injection of cisplatin (30 mg/kg), followed by blood urea nitrogen (*G*), serum creatinine (*H*), and histological analysis (*I*) at the indicated time points. *J*, representative H&E staining depicting renal tubular damage (indicated by an *asterisk*) linked with ischemia, cisplatin-nephrotoxicity, and rhabdomyolysis-associated AKI. In all the bar graphs ($n = 8$ biologically independent samples), experimental values are presented as mean ± S.D. The height of *error bar* = 1 S.D., and $p < 0.05$ was indicated as statistically significant. Student's *t* test (*A–I*) was carried out and statistical significance is indicated by $^{*}p < 0.05$, $^{**}p < 0.01$, $^{***}p < 0.001$. *Scale bar* (*J*): 100 μm.

Interestingly, the role of *Vgf* in kidney physiology and pathophysiology remains unknown. Here, using transcriptome profiling and RTEC-specific gene ablation studies, we report that *Vgf* is a stress-inducible gene that plays a protective role during the development of AKI.

Results

Mouse models of acute kidney injury

To identify common stress-induced cellular transcriptome changes linked to the pathogenesis of acute kidney injury, we sought to perform bulk RNA-seq of renal tissues from distinct murine models of AKI. To this end, we utilized the well-characterized mouse models of ischemia-reperfusion injury (IRI), drug-induced nephrotoxicity (cisplatin), and rhabdomyolysis-mediated kidney injury. IRI-associated AKI results from a generalized or localized impairment of oxygen and nutrient delivery to the kidneys (6). Cisplatin nephrotoxicity results from specific drug uptake (24) and direct toxicity to tubular epithelial cells. Rhabdomyolysis-associated AKI results from skeletal muscle injury and the subsequent myoglobin release into the systemic circulation, which causes renal dysfunction (3).

In these mouse models, bilateral ischemic surgery, intraperitoneal cisplatin injection, and intramuscular glycerol injection trigger AKI within 24–72 h. The development and progression of AKI was determined by accumulation of nitrogenous waste (blood urea nitrogen and serum creatinine) and histological analysis of tissue damage (H&E staining and renal damage score). During ischemia- (Fig. 1, *A–C*) and rhabdomyolysis-associated (Fig. 1, *D–F*) kidney injury, onset of renal impairment occurs 24 h post-surgery or -injection, whereas in the cisplatin-associated kidney injury models, renal impairment is observed 72 h post-injection (Fig. 1, *G–I*). Histological analysis revealed similar tubular damage in IRI (24 h), rhabdomyolysis (24 h), and cisplatin (72 h) groups (Fig. 1*J*).

Transcriptome profiling of AKI-associated differentially expressed genes

Because of temporal differences in the onset of kidney injury, we chose to compare gene expression signals at time points where the extent of kidney injury is similar in the three groups. To this end, we isolated renal tissues from control- (mock and vehicle, $n = 8$), IRI- (24 h, $n = 4$), rhabdomyolysis- (24 h, $n = 4$), and cisplatin-treated (72 h, $n = 4$) mice and then performed RNA-seq (4–8 biological replicates). Principal component analysis showed that the biological replicates clustered together across groups, signifying a high degree of similarity (Fig. 2*A*). Hierarchical clustering (Fig. 2*B*) revealed both divergent and convergent gene signatures between the control and the three AKI groups. In the three AKI conditions (false discovery rate (FDR) < 0.05 and fold change ≥ 2), we identified a common set

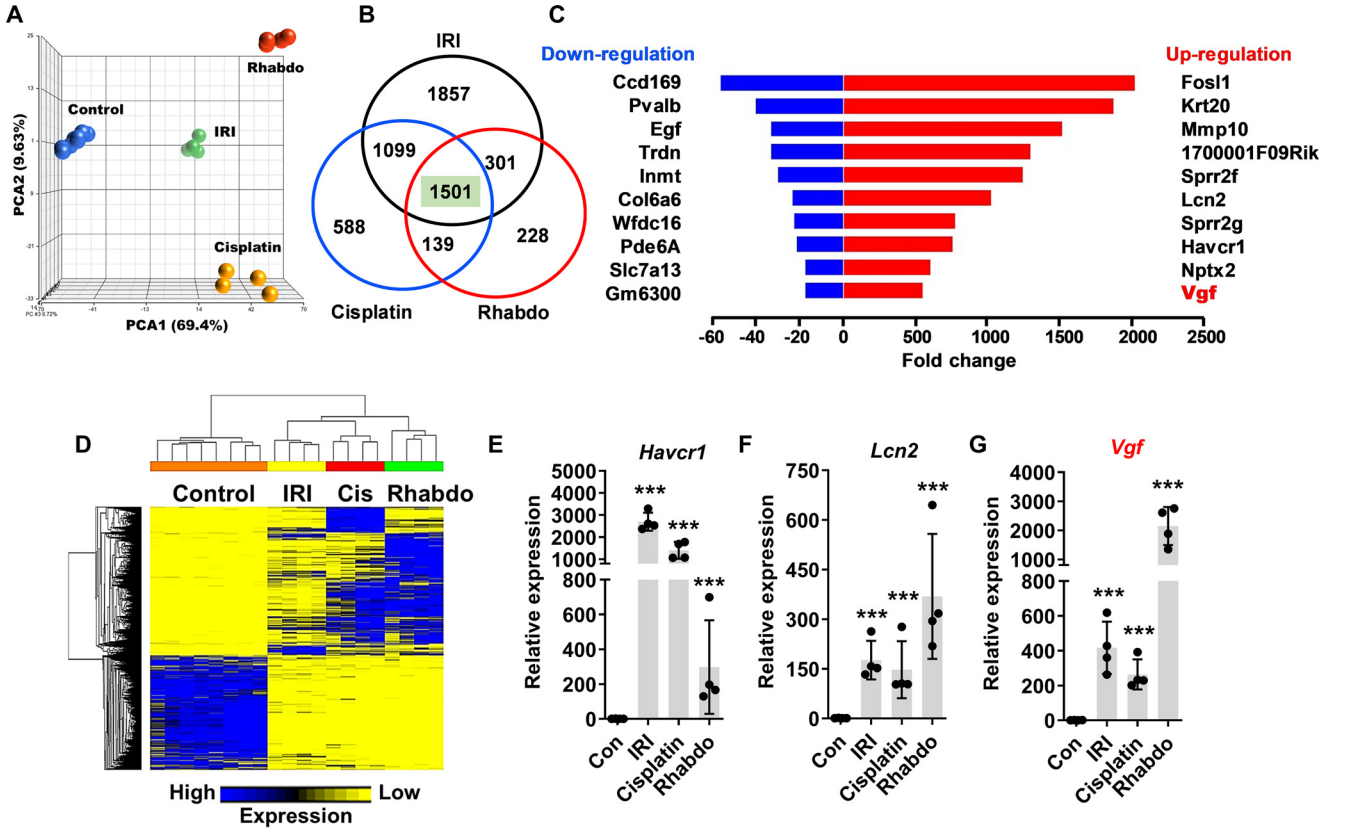

Figure 2. Transcriptome analysis of AKI-associated differentially expressed genes. Renal cortical tissues from control (mock and vehicle-treated) mice and mice undergoing AKI (IRI, cisplatin nephrotoxicity, and rhabdomyolysis) were utilized for transcriptome analysis. *A*, principal component analysis of bulk RNA-Seq data from control ($n = 8$) and AKI ($n = 4$) groups showed that biological replicates clustered together across groups, signifying a high degree of similarity. *B*, Venn diagram depicting common differentially expressed genes in the AKI groups. In the three AKI groups, a common set of 1501 genes were found to differentially expressed as compared with control group. *C*, graphical depiction of top up- and down-regulated genes in three distinct AKI models. *D*, heatmap of differentially expressed genes during AKI. *E–G*, gene expression analysis of *Havcr1*, *Lcn2*, *Vgf* genes showed injury-induced up-regulation. In all (*E–G*) the bar graphs ($n = 4$ biologically independent samples), experimental values are presented as mean ± S.D. The height of *error bar* = 1 S.D., and $p < 0.05$ was indicated as statistically significant. One-way ANOVA, followed by Dunnett's (*E–G*), was carried out, and statistical significance is indicated by $^{*}p < 0.05$, $^{**}p < 0.01$, $^{***}p < 0.001$.

of 1501 differentially expressed genes (771 genes were down-regulated and 709 genes were up-regulated) (Fig. 2*C*). In Supplemental Files 1 and 2, we have provided the complete list and normalized expression levels of all detected and differentially expressed genes. Enrichment of genes related to GSH, nicotinamide, and fatty acid metabolism were observed upon gene ontology (GO) and Kyoto Encyclopedia of Genes and Genomes (KEGG) pathway analysis (Supplemental File 3). These pathways have been recently probed for their role in renal dysfunction (25, 26).

To identify previously unexplored genes, we initially focused our attention on the top differentially expressed genes in the AKI conditions. The top common up-regulated genes in AKI mice were *Fosl1*, *Krt20*, *Mmp10*, *1700001F09Rik*, *Sprr2f*, *Lcn2*, *Sprr2g*, *Havcr1*, *Nptx2*, and *Vgf* (Fig. 2*D*). On the other hand, the top common down-regulated genes were *Ccdc169*, *Pvalb*, *Egf*, *Trdn*, *Inmt*, *Col6a6*, *Wfdc16*, *Pde6a*, *Slc7a13*, and *Gm6300*. The molecular functions of some of these differentially expressed genes, including the widely studied injury biomarkers Lcn2 and Havcr1, have been explored previously (27, 28). We found that similar to *Havcr1* and *Lcn2* up-regulation, 200–2000-fold induction of *Vgf* gene expression is observed in the three AKI conditions (Fig. 2, *E–G*). Immunoblot analysis showed a robust increase in Vgf protein levels early during the development of AKI (Fig. S1). These results indicated that *Vgf* is transcriptionally up-regulated in response to wide-ranging forms of renal injury.

Stress-induced Vgf up-regulation in RTECs during AKI

Vgf (nonacronymic) was first identified as a nerve growth factor–induced gene in a neuroendocrine cell line (18). The *Vgf* gene encodes a highly conserved precursor polypeptide of 615 (human) and 617 (rat and mice) amino acids. The precursor polypeptide contains several cleavage sites, and protease action at these locations results in the generation of a number of peptides, which exert pleotropic biological activities (19), including promotion of pro-survival signaling in an autocrine and paracrine fashion (29, 30). Although Vgf plays critical roles in neuronal and endocrine tissues, its role in the kidneys remains unknown.

We initially sought to validate the RNA-seq data and investigate the cellular origin of *Vgf* mRNA up-regulation. To do so, we used reporter mice (31) that expressed membrane-localized GFP in the tubular epithelial cells (Fig. 3*A*). These mice were challenged with ischemia, cisplatin, and rhabdomyolysis (Fig. S2), followed by isolation of GFP-positive cells from the kidneys

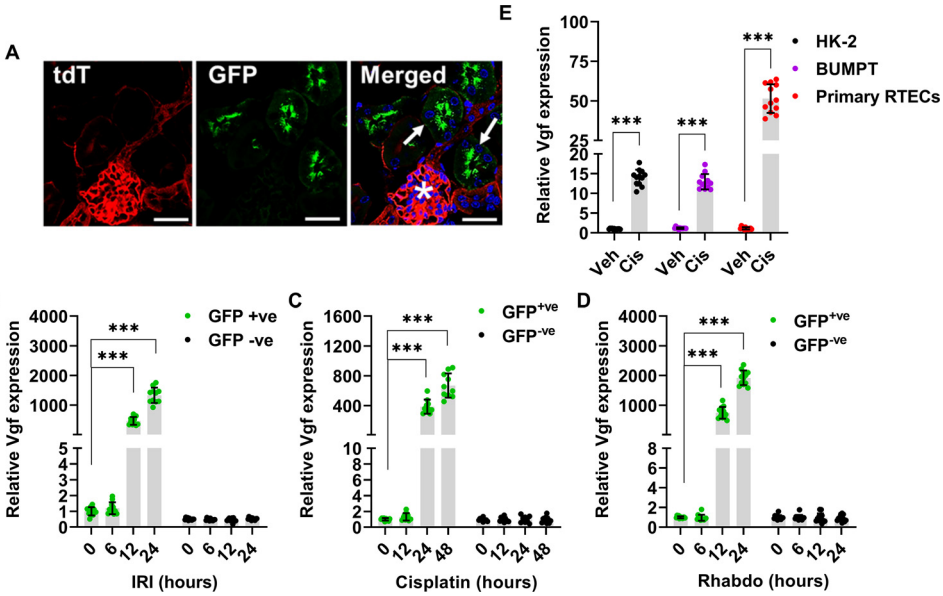

Figure 3. Vgf is up-regulated in the tubular epithelial cells during AKI. ROSAmT/mG were crossed with Ggt1-Cre mice to generate transgenic mice that express membrane-localized EGFP in renal tubular epithelial cells, whereas the other cell types express membrane-localized tdTomato. *A*, representative image showing EGFP expressing renal tubules (*arrows*) and tdTomato expression in the glomerulus (*asterisks*). *B–D*, renal *Vgf* expression was monitored at indicated time points using qPCR-based analysis. The results demonstrate *Vgf* gene induction during the early stages of AKI. *E*, human (HK-2) and murine (BUMPT) tubular epithelial cell lines and murine primary tubular epithelial cells were treated with either vehicle (PBS) or 50 μM cisplatin followed by gene expression analysis at 12 h. Cisplatin treatment *in vitro* resulted in *Vgf* mRNA induction in both the cell lines and primary tubular epithelial cells. In all the bar graphs (n = 10–11 biologically independent samples), experimental values are presented as mean ± S.D. The height of *error bar* = 1 S.D., and $p < 0.05$ was indicated as statistically significant. One-way ANOVA followed by Dunnett's (*B–D*) or Student's *t* test (*E*) was carried out, and statistical significance is indicated by $*p < 0.05$, $**p < 0.01$, $***p < 0.001$. *Scale bar* (*A*): 100 μM.

and subsequent examination of *Vgf* gene expression. We found that *Vgf* mRNA up-regulation occurs in RTECs (GFP-positive cells) early during the development of AKI (Fig. 3, *B–D*). A similar increase in *Vgf* expression was observed when human and murine RTEC cell lines (HK-2 and BUMPT cells) and primary murine RTECs were challenged with cisplatin under *in vitro* conditions (Fig. 3*E*). Based on these results, we concluded that *Vgf* up-regulation in RTECs is a common response to stress *in vitro* and *in vivo*.

Vgf gene deletion in renal tubular epithelial cells aggravates AKI

To probe the functional role of Vgf in the pathogenesis of AKI, we examined the effect of *Vgf* gene ablation on the severity of AKI. To this end, we generated *Vgf* conditional knockout ($Vgf^{PT-/-}$) mice by crossing the *Vgf*-floxed mice with the Ggt1-Cre mice. In Ggt1-Cre mice, Cre recombinase is expressed in RTECs 7–10 days after birth, and as a result Cre-mediated gene ablation is unlikely to influence normal renal development (32). $Vgf^{PT-/-}$ mice were indistinguishable from WT littermates and normal renal function was not evidently influenced by *Vgf* deficiency in RTECs (Fig. S3). Immunoblot and immunofluorescence experiments confirmed *Vgf* knockout in RTECs (Fig. 4, *A–C*). However, when the control and $Vgf^{PT-/-}$ littermates were challenged with ischemia, cisplatin, and rhabdomyolysis, we observed that *Vgf* gene deletion markedly exacerbates renal injury (Fig. 4, *D–I* and Fig. S4). To further corroborate these results, we cultured primary RTECs from the WT and $Vgf^{PT-/-}$ mice, challenged them with cisplatin, and then carried out viability assays. Cell survival and caspase assays (Fig. S5) showed that *Vgf* gene deletion results in increased cisplatin-induced cell death. Thus, we propose that Vgf plays a cytoprotective role in RTECs under stress conditions associated with AKI.

Vgf-associated TLQP-21 peptide protects RTECs under stress conditions

Vgf has several pleiotropic functions in neurons and endocrine cells (18). Notably, several Vgf proteolytic peptides have been identified and are named by the first four N-terminal amino acids and their total length (*e.g.* TLQP-62, TLQP-21, HHPD-41, AQEE-11, and LQEQ-19) (19). These peptides can influence various cellular processes, including activation of pro-survival signaling under stress conditions (29, 30, 33, 34). Some of the biological effects of these Vgf-associated peptides are believed to be mediated through binding to extracellular receptors such as the complement-binding protein gC1qR and complement C3a receptor 1 (C3AR1) (35, 36).

We found that TLQP-21 levels were increased in the renal tissues of WT mice challenged with ischemia-, cisplatin-, and rhabdomyolysis-associated AKI (Fig. 5*A*). Additionally, WT primary murine RTECs secreted TLQP-21 in the medium when challenged with cisplatin (Fig. 5*B*). Interestingly, tissue distribution studies in mice have shown that intravenously injected TLQP-21 markedly accumulates in the kidney (37). This prompted us to carry out *in vivo* "add-back" experiments to determine whether the TLQP-21 administration can reverse the aggravated renal impairment phenotype observed in the $Vgf^{PT-/-}$ mice. To this end, we administered a scrambled

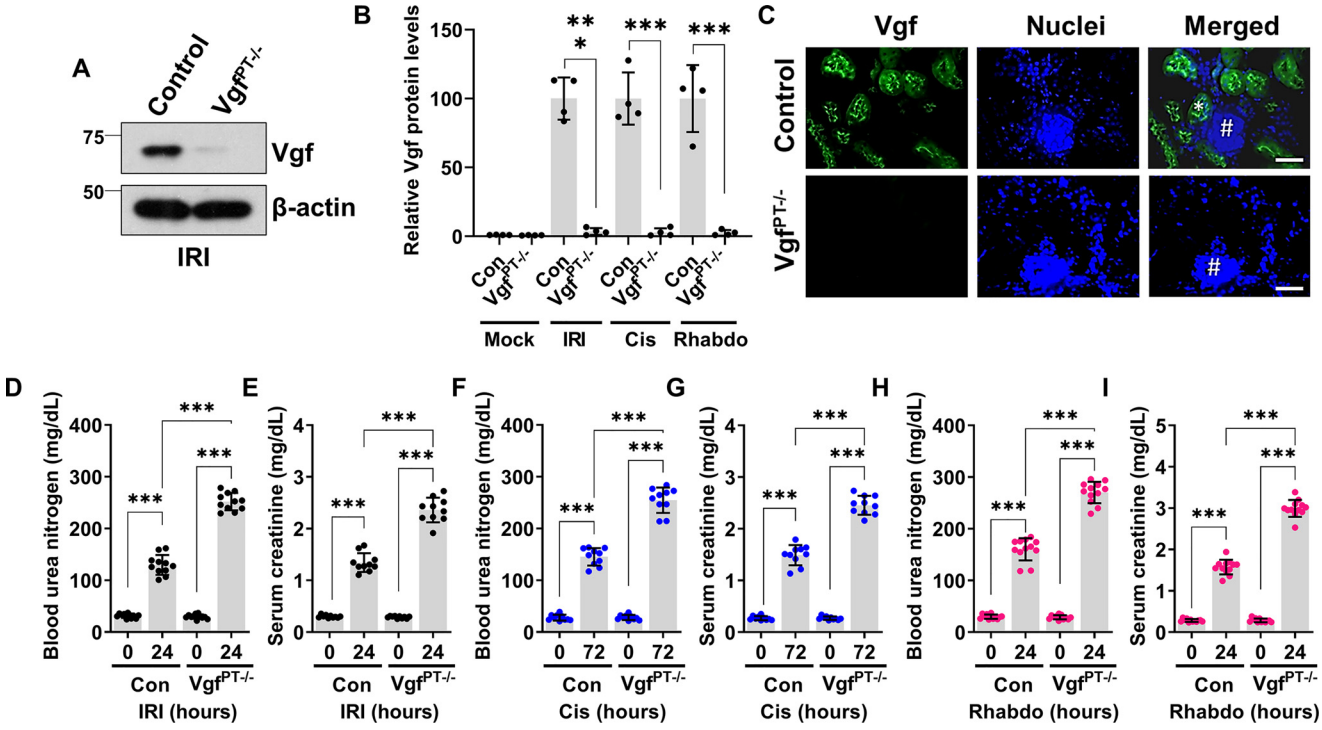

Figure 4. RTEC-specific Vgf gene ablation aggravates AKI. RTEC-specific *Vgf* knockout mice were generated by crossing Ggt1-Cre mice with *Vgf*-floxed mice. 8–12-week-old littermate control and *Vgf* conditional knockout male mice (indicated by $Vgf^{PT-/-}$) were then challenged with bilateral renal ischemia (30 min), cisplatin (30 mg/kg, single intraperitoneal injection) treatment, or glycerol-induced rhabdomyolysis (7.5 ml/kg 50% glycerol in the hind-leg muscles) followed by examination of renal structure and function. *A* and *B*, immunoblot analysis of Vgf protein levels was performed using renal cortical tissues from the control and *Vgf*-deficient mice followed by densitometric analysis (normalized to β-actin levels) using ImageJ. The graph depicts relative Vgf protein levels and shows successful gene knockout in the renal tissues. Blots are representative of three independent experiments. *C*, immunofluorescence analysis of renal cortical tissues from control and $Vgf^{PT-/-}$ mice challenged with IRI shows that Vgf staining is localized to cortical tubules (one positive tubule highlighted with *asterisks*) and no staining was observed in the glomerulus (marked with #). Blood urea nitrogen and serum creatinine analysis showed that tubular epithelial-specific *Vgf* deficiency results in aggravated renal impairment in the IRI- (*D* and *E*), cisplatin- (*F* and *G*), and rhabdomyolysis-associated (*H* and *I*) mouse models of AKI. In all the *bar graphs* (n = 4–11 biologically independent samples), experimental values are presented as mean ± S.D. The height of *error bar* = 1 S.D., and $p < 0.05$ was indicated as statistically significant. One-way ANOVA followed by Tukey's multiple-comparison test (*A–I*) was carried out, and statistical significance is indicated by $*p < 0.05$, $**p < 0.01$, $***p < 0.001$. *Scale bar* (*C*): 100 μm.

peptide or TLQP-21 to control and $Vgf^{PT-/-}$ mice at 24 and 48 h after challenging them with cisplatin (Fig. 5*C*). Remarkably, we found that TLQP-21 administration mitigates cisplatin-associated AKI in the $Vgf^{PT-/-}$ mice (Fig. 5, *D–F*), indicating that loss of TLQP-21 might be partly responsible for the increased sensitivity to renal injury. Complementary studies in primary murine RTECs showed that TLQP-21 treatment can protect *Vgf*-deficient RTECs from cisplatin-induced cell death (Fig. S6). These results indicate that the loss of TLQP-21 is partly responsible for the aggravated renal impairment phenotype seen in the *Vgf*-deficient mice.

VGF regulation by Sox9 in the early acute phase of renal injury

Next, we sought to identify the transcriptional mechanisms underlying stress-induced *Vgf* up-regulation in RTECs. While exploring the transcription factor binding sites in the *Vgf* promoter, we noticed the presence of a putative Sox9 binding site (Fig. 6*A*). Sox9 is up-regulated in RTECs in response to injury and is a critical transcriptional regulator of epithelial cell fate during AKI (31, 38–41). To test the hypothesis that Sox9 is involved in *Vgf* up-regulation during AKI, we performed promoter-driven luciferase-based reporter assays (Fig. 6*B*) in HEK293 cells, which have low endogenous Sox9 expression. To this end, we used HEK293 cells with stable vector transfection (low Sox9) and Sox9 overexpression (high Sox9) for *Vgf* promoter–driven luciferase reporter assays as described in our recent study (31). We found that Sox9 increases *Vgf* promoter activity (Fig. 6*C*). Importantly, site-directed mutagenesis of a Sox9 binding site within the *Vgf* promoter suppressed promoter activity. To substantiate these findings, we performed ChIP analysis, which confirmed Sox9 binding at the *Vgf* promoter *in vivo* (Fig. 6*D*).

We next asked if RTEC-specific Sox9 deficiency influences stress-responsive *Vgf* up-regulation. Our recent study (31) revealed a protective role of Sox9 during ischemic and nephrotoxic AKI. We also found that RTEC-specific Sox9 gene deletion aggravates rhabdomyolysis-associated AKI (Fig. S7). When we carried out gene expression analysis of renal tissues from control and $Sox9^{PT-/-}$ mice, we found that stress-induced *Vgf* up-regulation is Sox9 dependent (Fig. 6, *E–G*). Sox9-deficient mice had greater than 95% reduction in *Vgf* mRNA levels. Furthermore, immunoblot analysis in control and Sox9-deficient renal tissues showed that injury-induced Vgf up-regulation is Sox9 dependent (Fig. 6*H*). Taken together, these data indicate that Sox9 controls *Vgf* gene transcription in RTECs during AKI.

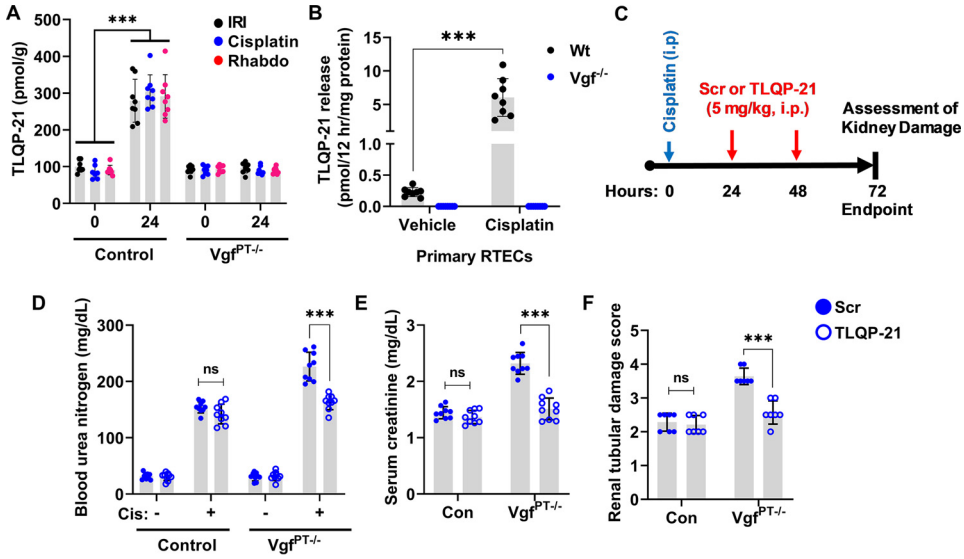

Figure 5. Renal protective effects of Vgf-derived peptide TLQP-21. *A*, kidney cortical tissue lysates from mock treated mice (0 h) or mice undergoing AKI (IRI, cisplatin, and rhabdomyolysis, 24 h) were used for measurement of TLQP-21 levels using an ELISA-based assay. More than 2-fold increase in TLQP-21 levels was observed in the control mice undergoing AKI. *Asterisk* indicates statistical significance as compared with respective mock or vehicle treated (0 h) group. *B*, primary murine renal tubular cells of indicated genotypes were treated with 50 μM cisplatin, and levels of TLQP-21 secreted in the media were assessed by an ELISA-based method. Cisplatin treatment resulted in TLQP-21 release into the media 12 h post cisplatin treatment in the WT RTECs. *C*, littermate control and $Vgf^{PT-/-}$ mice were treated with cisplatin (30 mg/kg) on day 0, followed by intraperitoneal injection of either a scrambled peptide or TLQP-21 (5 mg/kg in normal saline) on days 1 and 2. Renal damage was then examined on day 3. Blood urea nitrogen (*D*), serum creatinine (*E*), and histological analysis (*F*) showed that the TLQP-21 administration can partly reverse the aggravated cisplatin nephrotoxicity seen in the $Vgf^{PT-/-}$ mice. In all the bar graphs (n = 8–9 biologically independent samples), experimental values are presented as mean ± S.D. The height of *error bar* = 1 S.D., and $p < 0.05$ was indicated as statistically significant. One-way ANOVA followed by Dunnett's was carried out, and statistical significance is indicated by $^{*}p < 0.05$, $^{**}p < 0.01$, $^{***}p < 0.001$.

The Sox9-Vgf axis is conserved in human RTECs

We next investigated the Sox9-Vgf axis in a human RTEC cell line (HK-2). In these cells, cisplatin treatment resulted in Vgf protein induction, which we were able to suppress by transfecting the cells with two *Vgf*-specific siRNAs (Fig. 7*A*). We then examined the effect of *Vgf* knockdown on cellular sensitivity to cisplatin. Cell survival and caspase assays showed that *Vgf* knockdown results in increased cell death in response to cisplatin treatment (Fig. 7, *B–D*). We subsequently explored the role of Sox9 in cisplatin-induced *Vgf* up-regulation. To this end, we transfected HK-2 cells with control or Sox9-targeting siRNAs, followed by cisplatin treatment. Immunoblot analysis confirmed RNAi-mediated Sox9 knockdown (Fig. 7*E*). It also showed that cisplatin-mediated Vgf up-regulation was Sox9-dependent (Fig. 7*E*). Importantly, gene expression analysis confirmed that Sox9 knockdown suppresses *Vgf* mRNA up-regulation (Fig. 7*F*). Furthermore, bioinformatics analysis identified a putative Sox9 target site in the human *Vgf* promoter (Fig. 7*G*). Promoter-based luciferase assay showed that Sox9 increases *Vgf* promoter activity, which was inhibited when the Sox9 binding site was mutated (Fig. 7*H*). Finally, *Vgf* up-regulation in response to injury was confirmed in a porcine model of ischemia AKI (42) and a human organoid (43, 44) model of cisplatin-associated injury (Fig. S8). Collectively, these studies with multiple mouse models of AKI, primary murine RTECs, human RTEC cell line (HK-2), porcine AKI model, and human organoids suggest that stress-mediated *Vgf* up-regulation is likely a conserved and protective mechanism in RTECs.

Discussion

Here we have mapped the transcriptome changes accompanying the development of ischemic, nephrotoxic, and rhabdomyolysis-associated acute kidney injury. We find that these diverse stress conditions trigger transcriptional up-regulation of *Vgf* gene in renal tubular epithelial cells. Importantly, we provide functional evidence that Sox9-mediated *Vgf* up-regulation protects RTECs from cell death and dysfunction linked with AKI. These findings identify *Vgf* as an essential stress-responsive and protective gene in kidney epithelial cells.

Spatial and temporal changes in gene expression in response to ischemia reperfusion–associated kidney injury has been comprehensively explored (39, 45). Because multiple etiologies can contribute to the development of AKI, in the current study, we aimed to identify common transcriptional changes that occur in the acute phase of three distinct murine models of AKI. Consistent with previous studies (39, 45), we observed that genes such as Sprr2f and Krt20 and well-characterized renal injury biomarkers such as Lcn2 and Havcr1 were significantly up-regulated during ischemic, nephrotoxic, and rhabdomyolysis-associated acute kidney injury. Furthermore, pathway enrichment analysis revealed that genes linked to cell death and survival, wound healing, small molecule and fatty acid metabolism, and molecular transport were differentially expressed during AKI.

Vgf was among the top up-regulated genes in the renal tissues of mice undergoing ischemic, nephrotoxic, and rhabdomyolysis-associated AKI. The *Vgf* gene is known to be expressed in a subset of cells in the central and peripheral nervous system and endocrine cells in the adrenal gland, gastrointestinal tract, and

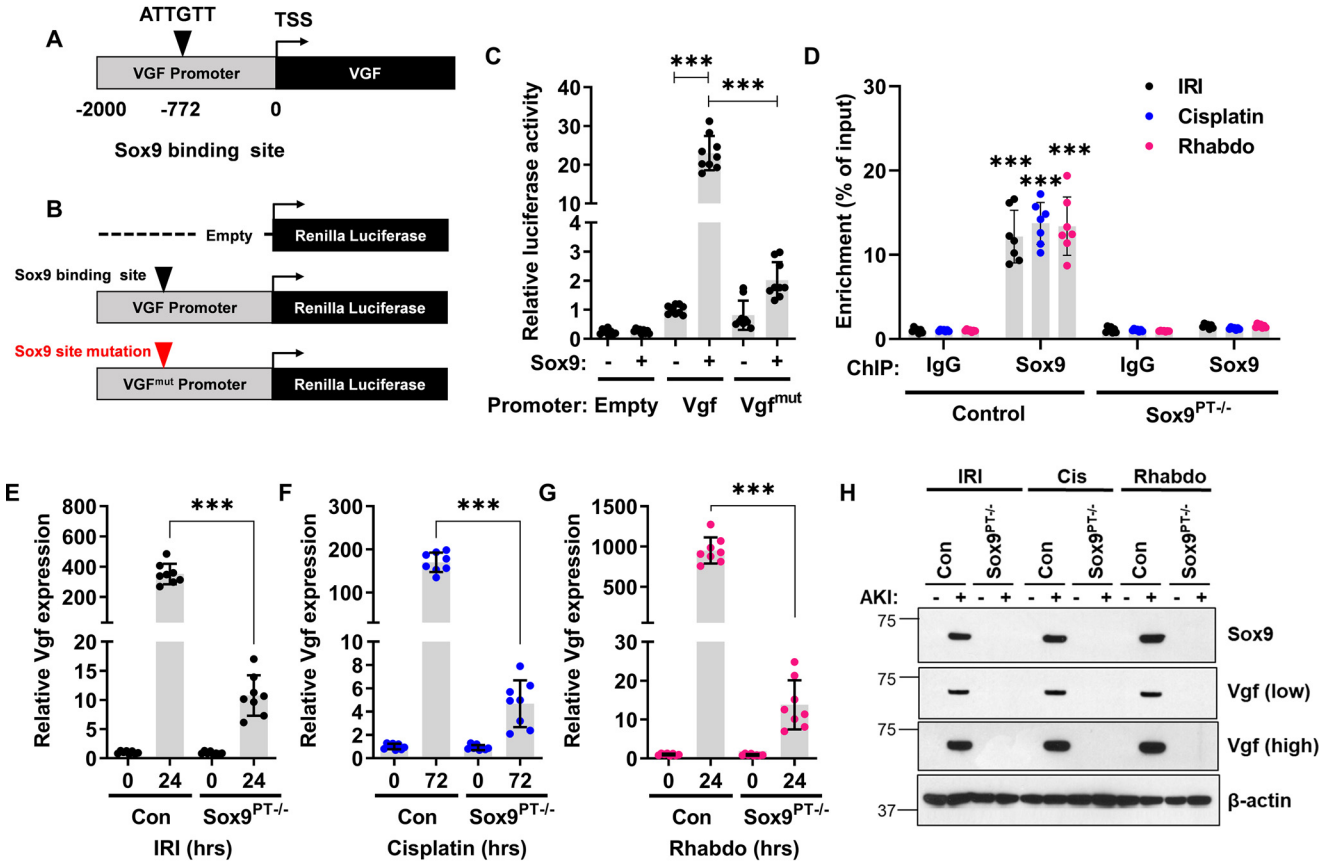

Figure 6. Vgf is a Sox9 target gene. *A*, schematic representation of murine *Vgf* promoter, highlighting the putative Sox9 binding site. *B* and *C*, HEK293 cells were stably transfected with empty plasmid or Sox9 construct. The mock transfected cells (−) and Sox9 expressing cells (+) were then used for luciferase-based reporter assays. The *Vgf* promoter sequences (−2000bp from transcription start site (TSS)) was cloned in a luciferase reporter construct. Mock (−) and Sox9 (+) expressing cells were transiently co-transfected with reporter Renilla luciferase constructs (empty, Vgf, or Vgf^{mut}) and reference Cypridina luciferase (normalizing control), followed by measurement of luciferase activity at 24 h. The normalized luciferase activity of mock (−) group was then compared with the Sox9 (+) group. The results show that the Sox9 can activate transcription from the *Vgf* promoter. In the Vgf^{mut} construct, the Sox9 binding site was mutated from ATTGTT to AACAAT. *D*, Sox9 ChIPs were carried out from the renal tissues of control and $Sox9^{PT-/-}$ mice undergoing ischemia-, cisplatin nephrotoxicity-, and rhabdomyolysis-associated AKI. Subsequent qPCR analysis using primers specific for the murine *Vgf* promoter region showed that Sox9 can bind to *Vgf* promoter *in vivo*. *E–G*, qPCR-based gene expression analysis was carried out in the renal tissues from littermate control and $Sox9^{PT-/-}$ mice at indicated time points after induction of kidney injury. The injury-induced *Vgf* mRNA up-regulation was suppressed in the $Sox9^{PT-/-}$ mice. *H*, immunoblot analysis of renal cortical tissues showed that AKI-induced Vgf protein induction is suppressed in the $Sox9^{PT-/-}$ mice. Blots are representative of three independent experiments. In all the bar graphs (n = 8–9 biologically independent samples), experimental values are presented as mean ± S.D. The height of *error bar* = 1 S.D., and $p < 0.05$ was indicated as statistically significant. One-way ANOVA followed by Tukey's (*C*) or Dunnett's (*D–G*) multiple-comparison test was carried out, and statistical significance is indicated by $*p < 0.05$, $**p < 0.01$, $***p < 0.001$.

pancreas (18). Within the nervous system, *Vgf* expression is rapidly induced by neurotrophins, synaptic activity, nerve injury, inflammation, and other stimuli (21). Consistent with its expression in the central and peripheral nervous system, Vgf has been implicated in the regulation of neuroplasticity associated with learning, memory, depression, and chronic pain (21, 46, 47). Additionally, Vgf plays a critical role in energy homeostasis and metabolism (23, 34, 48). Mice with germline *Vgf* deletion are lean, hyper-metabolic, and resistant to diet-, lesion-, and genetically induced obesity and diabetes (20). Interestingly, the role of Vgf in renal physiology and pathology has remained unexplored.

We found that *Vgf* expression was low in the normal adult kidneys. Moreover, renal epithelial cell–specific *Vgf* deficiency did not have any deleterious effect on the normal kidney structure or function and did not alter the overall body weight. Importantly, *Vgf* expression increased by more than 500-fold in RTECs during ischemic, nephrotoxic, and rhabdomyolysis-associated AKI. A previous study (39) also described *Vgf* gene induction during IRI; however, its functional role in the pathogenesis remained unknown. We find that RTEC-specific *Vgf* deletion markedly aggravated renal impairment linked with ischemic, nephrotoxic, and rhabdomyolysis-associated AKI. Notably, stress-responsive *Vgf* up-regulation was recapitulated in human and murine cell culture models of cisplatin-associated cellular injury. Functional studies also showed that *Vgf* deficiency sensitizes RTECs to cisplatin-mediated cell death. These studies reveal that Vgf protects RTECs from cell death and dysfunction.

The neuroendocrine functions attributed to the *Vgf* gene are dependent on the post-translational processing of Vgf polypeptide into various bioactive peptides, such as TLQP-21, TLQP-62, AQEE-30, LQEQ-19, and NERP2. Among these, TLQP-21 is known to control regulatory processes involved in energy expenditure, lipolysis, glucose-stimulated insulin secretion, gastric acid secretion, and pain (34, 47, 49). We found that along

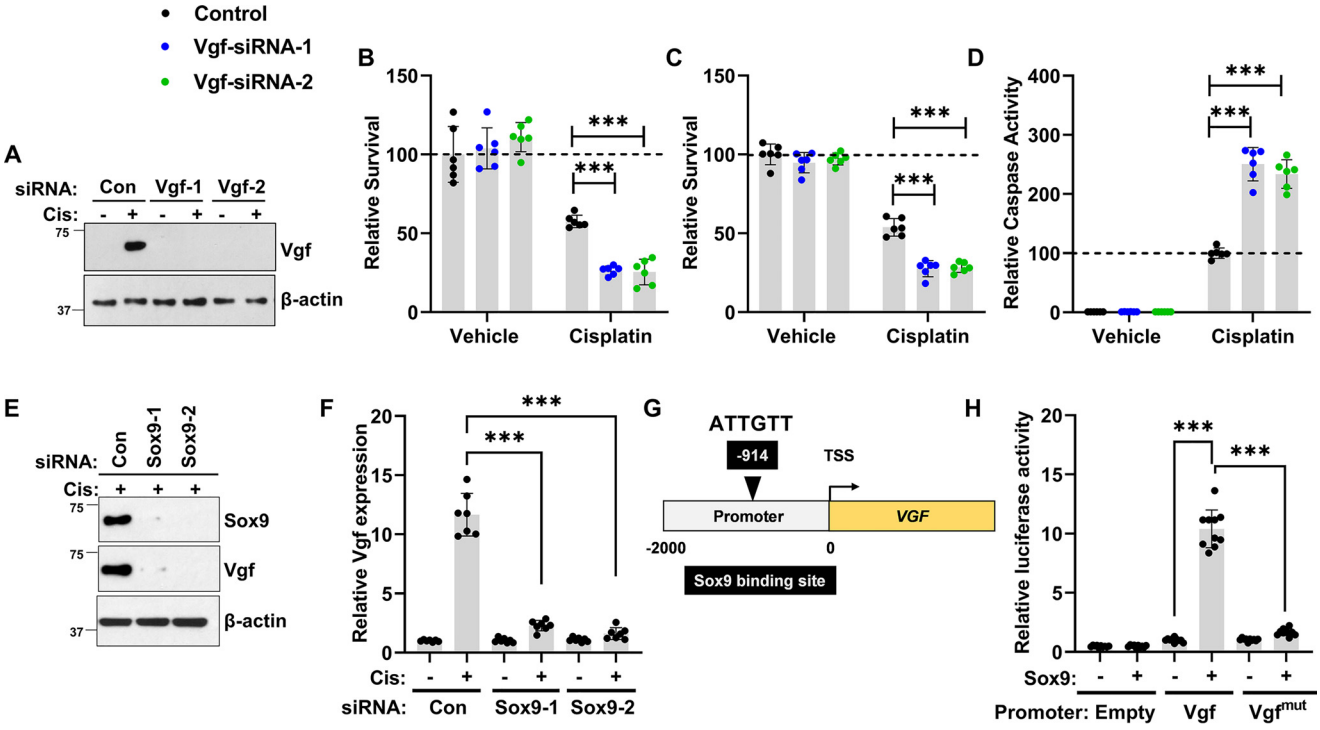

Figure 7. Stress-induced Sox9-Vgf axis in human RTECs. HK-2, a renal tubular epithelial cell line derived from normal human kidney, was used to examine the Sox9-Vgf axis. *A*, HK-2 cells were transiently transfected with control or two distinct *Vgf*-targeting siRNA constructs, followed by cisplatin treatment. Immunoblot analysis showed that cisplatin treatment results in Vgf protein induction, which was significantly blocked by both the *Vgf*-targeting siRNAs. Measurement of cellular viability by (*B*) trypan blue staining, (*C*) MTT assay, and (*D*) caspase activity showed that *Vgf* knockdown sensitizes HK-2 cells to cisplatin-associated cell death. *E*, to examine the role of Sox9 in cisplatin-associated *Vgf* gene induction, we used RNAi-based knockdown of Sox9 in HK-2 cells. HK-2 cells were transiently transfected with control or two distinct Sox9-targeting siRNA constructs, followed by cisplatin treatment. Immunoblot analysis showed that Sox9-targeting siRNAs successfully knocked down Sox9 protein levels. *F*, qPCR-based gene expression analysis showed that RNAi-mediated Sox9 knockdown suppressed cisplatin-mediated *Vgf* mRNA up-regulation. *G*, schematic representation of human *Vgf* promoter, highlighting the putative Sox9 binding site. *H*, HEK293 cells were stably transfected with empty plasmid or Sox9 construct. The mock transfected cells (−) and Sox9-expressing cells (+) were then used for luciferase-based reporter assays. The *Vgf* promoter sequences (−2000bp from transcription start site (TSS)) was cloned in a luciferase reporter construct. Mock (−) and Sox9 (+)-expressing cells were transiently co-transfected with reporter Renilla luciferase constructs (empty, Vgf, or Vgf^{mut}) and reference Cypridina luciferase (normalizing control), followed by measurement of luciferase activity at 24 h. The results show that the Sox9 can activate transcription from the *Vgf* promoter. In the Vgf^{mut} construct, the Sox9 binding site was mutated from ATTGTT to AACAAT. In all the bar graphs (n = 6–10 biologically independent samples), experimental values are presented as mean ± S.D. The height of *error bar* = 1 S.D., and $p < 0.05$ was indicated as statistically significant. One-way ANOVA, followed by Tukey's multiple-comparison test, was carried out, and statistical significance is indicated by $^{*}p < 0.05$, $^{**}p < 0.01$, $^{***}p < 0.001$.

with *Vgf* mRNA, TLQP-21 levels also increase in the renal tissues during AKI. Strikingly, systemic TLQP-21 administration partly reversed the injury-induced aggravation of renal impairment observed in the RTEC-specific *Vgf*-deficient mice. These findings suggest that Vgf-derived TLQP-21 plays a protective role during AKI. A critical feature of Vgf peptides is their cell type–specific diversity in tissues studied so far and their selective modulation in response to organ or cell type–relevant stimuli (19). Future studies are thus necessary to comprehensively profile Vgf-derived peptides in renal tissues under normal and stress conditions.

The underlying signaling mechanisms associated with the myriad neuroendocrine functions of Vgf remains incompletely understood. At least some of the biological functions of Vgf-derived peptides are mediated through extracellular receptor binding. Indeed, complement C3aR1 has been identified as a TLQP-21 receptor on microglia and other cell types (35, 50–52). For example, in the adipose tissue, TLQP-21 exerts an anti-obesity effect in diet-induced obese mice through binding to C3aR1 and inducing β-adrenergic receptor expression (53). Furthermore, C1qR, the globular head of the C1q receptor, has been identified as a TLQP-21 receptor in macrophages (36). Interestingly, a previous study demonstrated that C3aR1 is expressed in RTECs and that germline C3aR1 gene ablation provides protection from ischemia-associated AKI (54). It is well-established that complement activation within the injured kidneys triggers downstream inflammatory events within the renal parenchyma that exacerbate renal cell dysfunction and cell death (55, 56). Future studies with cell type–specific conditional knockout mice are required to tease out the possible role of C3aR1, C1qR, or other proteins as receptors of Vgf-derived peptides in the kidney.

How *Vgf* protects renal epithelial cells under stress conditions *in vivo* remains unclear. Our studies with cultured primary epithelial cells suggest that stress conditions trigger the induction of Vgf-derived TLQP-21, which might function in an autocrine and/or paracrine manner to protect RTECs from cisplatin-associated cell death. However, these epithelial cell culture models of injury do not completely recapitulate the *in vivo* pathophysiological complexities of AKI, particularly the involvement of other cell types such as immune cells (57–59). Therefore, our studies do not rule out the possibility that Vgf and TLQP-21 might influence renal injury through cross-talk

between epithelial and immune cells. Interestingly, in peripheral neurons, inflammatory conditions can cause *Vgf* up-regulation and Vgf can in turn functionally regulate inflammatory processes (60). Altogether, our study provides strong evidence for the protective role of RTEC-derived Vgf in AKI; however, the further unraveling of this pathway will require the identification of underlying receptors, modulated cell types, and intracellular signaling pathways.

Although the downstream pathways remain unclear, we propose that Sox9 is the critical transcriptional regulator of stress-induced *Vgf* up-regulation in RTECs. Several lines of evidence suggest that Sox9 directly binds to the *Vgf* promoter and promotes the transcriptional up-regulation of the *Vgf* gene. First, injury-induced *Vgf* up-regulation was significantly suppressed in renal tissues of RTEC-specific conditional *Sox9* knockout mice. Second, ChIP studies showed Sox9 enrichment at the *Vgf* promoter site *in vivo*. Third, luciferase reporter assays confirmed Sox9-mediated transactivation of the *Vgf* promoter, which was suppressed by mutations in the Sox9 binding site. These results establish *Vgf* as a *bona fide* Sox9 target gene in RTECs.

In the current study, we found that *Vgf* deficiency exacerbates AKI, a phenotype that is similar to the RTEC-specific Sox9-deficient mice (31). However, Sox9 is a crucial transcriptional regulator of not only the early pathogenic phase (31) but also the later recovery phase of AKI (38, 40). Sox9-expressing RTECs are involved in the repair and regeneration processes post-AKI (38, 40). Based on our findings that *Vgf* is a downstream Sox9 target gene, it will be interesting to examine whether Vgf contributes to repair and regeneration. It would also be interesting to examine whether the systemic TLQP-21 administration can accelerate the recovery and repair processes post-AKI. Collectively, our study has revealed *Vgf* as an essential Sox9 target gene that protects RTECs under stress conditions associated with acute kidney injury.

Experimental procedures

Cell culture and reagents

Boston University mouse proximal tubule cells (BUMPT, clone 306, generated by Drs. Wilfred Lieberthal and John Schwartz, Boston University School of Medicine, Boston, MA; obtained from Dr. Zheng Dong, Augusta University, Augusta, GA) were grown at 37 °C in DMEM with 10% FBS. The human renal tubular cell line, HK-2, cells (ATCC, CRL-2190) were grown in keratinocyte media according to the provider's instructions. HEK293 cells stably transfected with empty vector (pCMV6) or Sox9 expression vector have been described in our previous study (31) and were grown at 37 °C in DMEM with 10% FBS. Cisplatin, glycerol, TLQP-21 (murine), and other reagents were obtained from Sigma-Aldrich.

Primary murine tubular cell culture

Murine renal cortical tissues were minced and digested with 0.75 mg/ml collagenase IV (Thermo Fisher Scientific). The cells were centrifuged at 2000 × *g* for 10 min in DMEM/F-12 medium with 32% Percoll (Amersham Biosciences). After two washes with serum-free media, the cells were plated in collagen-coated dishes and cultured in DMEM/F-12 medium supplemented with 5 μg/ml transferrin, 5 μg/ml insulin, 0.05 μM hydrocortisone, and 50 μM vitamin C (Sigma-Aldrich). Fresh media was supplemented every alternate day, and after 5–7 days of growth, the isolated proximal tubular cells were trypsinized and replated at 1×10^5 cells/well in 24-well plates. To induce cell death, primary RTECs were incubated with 50 μM cisplatin (Sigma-Aldrich) in fresh culture medium for 24 h, followed by viability and caspase assays.

siRNA transfection, cell viability and caspase assays

Transient transfections and cell viability assays were performed according to methods described in our previous study (31). Briefly, the HK-2 cells were plated in 24- or 96-well plates and reverse-transfected with 25 nM siRNA (Sigma-Aldrich) using Lipofectamine RNAiMAX reagent (Life Technologies). At 48 h post transfection, the cells were treated with 50 μM cisplatin in fresh media. Subsequently, 48 h posttreatment, cell viability assays and immunoblot analysis were performed. At the end of the incubation period, cells from 24-well plates were harvested, followed by trypan blue staining and manual cell counting with a hemocytometer and/or by using the Countess Automated Cell Counter (Thermo Fisher Scientific); translucent cells were considered as viable and blue-stained cells were counted as dead. Cellular viability was calculated by dividing the number of viable cells by the total cell number, and each sample was done in triplicate. For MTT assays, after cisplatin treatment in 96-well plates, 10 μl of MTT reagent (5 mg/ml MTT in PBS) was added to each well, and plates were incubated at 37 °C with 5% CO_2 for 4 h, followed by addition of 100 μl of acidified isopropanol (Sigma-Aldrich) and measurement of absorbance at 590 nm. The IC_{50} was calculated by nonlinear regression analysis using GraphPad Prism.

For caspase assays (61), the cells were lysed in a buffer containing 1% Triton X-100, and 10 μg of protein from cell lysates was added to an enzymatic assay buffer containing 50 μM DEVD-AFC for 60 min at 37 °C. Fluorescence at excitation 360 nm/emission 535 nm was measured, and free AFC was used to plot a standard curve. Subsequently, the standard curve was used to convert the fluorescence reading from the enzymatic reaction into the nM AFC liberated/mg protein/hour as a measure of caspase activity.

Mice strains and breeding

Mice were housed in a temperature-controlled environment with a 12-h light cycle and were given a standard diet and water *ad libitum*. All animal experiments were carried out in accordance with the animal use protocol approved by the Institutional Animal Care and Use Committee of the Ohio State University. C57BL/6J mice, *Vgf*-floxed mice, *Sox9*-floxed mice, and Ggt1-Cre transgenic mice (stock numbers 000664, 030571, 013106, and 012841, respectively) were obtained from Jackson Laboratories. *Vgf*-floxed mice and *Sox9*-floxed mice were bred with Ggt1-Cre transgenic mice to generate conditional gene knockout mice in renal tubular epithelial cells. These transgenic mice express Cre recombinase in the renal tubular epithelial cells beginning at age 1–2 weeks. mT/mG mice that express

membrane-targeted, two-color fluorescent Cre-reporter allele were obtained from Jackson Laboratories (stock 007676). The mT/mG mice were bred with Ggt1-Cre strain as reported previously (31). For all mouse colonies, the pups were ear-tagged and genotyped at 3 weeks of age. Offspring were genotyped by standard PCR-based methods. Primers used for amplification were *Vgf36100* (5′-TCCTCCCTCTCAGTGTTTGC-3′) and *Vgf36101* (5′-GGACTCGCACAAACCACAC-3′) and produced a 313-bp product for the *Vgf*-floxed allele and a 194-bp product for the *Vgf* WT allele. *Sox9-11576* (5′-AGACTCTGGGCAAGCTCTGG-3′) and *Sox9-11577* (5′-GTCATATTCACGCCCCCATT-3′) were used for amplification and yielded a 300-bp product for *Sox9*-floxed allele and a 250-bp product for the *Sox9* WT allele. Primers for Ggt1-Cre are Cre5′ (AGGTGTAGAGAAGGCACTTAGC) and Cre3′ (CTAATCGCCATCTTCCAGCAGG), which produce a 405-bp product. PCR products were analyzed by electrophoresis using 1.5% agarose gels.

Animal models of acute kidney injury

We carried out all the studies presented here in age-matched male mice at 8–12 weeks of age using methods described in our recent studies (31, 62, 63). In all the studies with conditional *Vgf* and *Sox9* knockout mice, we used male littermates from mice bred in-house. Experiments were carried out in a blinded fashion where the investigators assessing, measuring, or quantifying experimental outcomes were blinded to the genotype or treatment of the mice. For ischemia-reperfusion experiments, mice were anesthetized by isoflurane and placed on a surgical platform where the body temperature was monitored throughout the procedure. The skin was disinfected, kidneys were exposed, and bilateral renal pedicles were clamped for 30 min. Consequently, the clamps were removed to initiate reperfusion followed by suturing to close the muscle and skin around the incision. To compensate for the fluid loss, 0.5 ml of warm sterile saline was administered via intraperitoneal injection. Blood was collected on day 1 via cardiac puncture after carbon dioxide asphyxiation. Renal tissues were collected and processed for RNA-seq, qPCR, and histological analysis as described previously. For nephrotoxicity experiments, cisplatin (30 mg/kg) was administered by i.p. injection as described previously. After cisplatin injection, blood was collected on days 0–3 by submandibular vein bleed or on day 3 via cardiac puncture after carbon dioxide asphyxiation. Renal tissues were collected and processed for RNA-seq, qPCR, and histological analysis. To induce rhabdomyolysis, 8–12-week-old male mice were injected with 7.5 ml/kg 50% glycerol intramuscularly to the two hind-legs or injected with saline as a control, followed by tissue collection at 24 h and RNA-seq, qPCR, and histological analysis. The porcine model of ischemic AKI has been described previously (42). We utilized the renal cortical tissues from porcine kidneys for qPCR-based analysis of *Sox9* and *Vgf* genes.

Assessment of renal damage

Renal damage was assessed by serum analysis (blood urea nitrogen and creatinine) and histological examination (H&E staining). Mouse blood samples were collected at indicated time points, followed by blood urea nitrogen and creatinine measurement by QuantiChrom™ Urea Assay Kit (DIUR-100) and Creatinine Colorimetric Assay Kit (Cayman Chemical Company). For histological analysis, mouse kidneys were harvested and embedded in paraffin at indicated time points before and after AKI induction. Tissue sections (5 μm) were stained with hematoxylin and eosin by standard methods (63). Histopathologic scoring was conducted in a blinded fashion by examining 10 consecutive 100× fields per section from at least three mice per group. Tubular damage was scored by calculation of the percentage of tubules that showed dilation, epithelium flattening, cast formation, loss of brush border and nuclei, and denudation of the basement membrane. The degree of tissue damage was scored based on the percentage of damaged tubules as previously described: 0, no damage; 1, <25%; 2, 25–50%; 3, 50–75%; and 4, >75%.

RNA-seq

Total RNA was isolated from harvested renal cortical tissues using the RNeasy Plus Mini Kit (Qiagen) according to the manufacturer's protocols. Total RNA samples used for library construction and sequencing (Quick Biology, Pasadena, CA). RNA integrity, quality, and purity were analyzed with an Agilent 2100 Bioanalyzer. Libraries for RNA-seq were prepared with KAPA Stranded mRNA-Seq Kit (KAPA Biosystems, Wilmington, MA) according to the manufacturer's protocols. The workflow consisted of mRNA enrichment using bead capture for poly(A) selection, cDNA generation, end repair to generate blunt ends, A-tailing, adaptor ligation, and PCR amplification of library fragments. Final Library size distribution was determined by using an Agilent 2100 Bioanalyzer using the High-Sensitivity DNA Kit, and its quantity was analyzed by Life Technologies Qubit 3.0 Fluorometer. Libraries were pooled and sequenced on the Illumina HiSeq 4000 platform to obtain 150-bp paired-end reads, 20 million reads (10 million reads pairs) per sample.

Bioinformatics analysis

Sequencing data quality checks were performed by using FastQC followed by read alignments using Bowtie2 version 2.1.0 with alignment to the mouse Ensembl genome (GRCm38/mm10). The overall mapping rate of more than 80% and rRNA percentage less than 5% was considered as good-quality mapping data. The reads were first mapped to the latest UCSC transcript set using Bowtie2 (version 2.1.0), and the gene expression level was estimated using RSEM v1.2.15. Differentially expressed genes were called for each time point with Bioconductor edgeR. TMM (trimmed mean of M-values) method in edgeR package was used to normalize the gene expression results. For all the analyses, we only kept genes with (*a*) false discovery rate (FDR)-transformed p values below 0.05, (*b*) fold change of at least 1.5, and (*c*) TMM above 1 in three distinct AKI and/or control samples. These values of fold change and TMM thresholds were chosen to enable experimental validation of our differential-expression calls. We used the fold changes calculated by edgeR to create a pre-ranked gene list.

Each list of differentially expressed genes derived from the different comparisons were subjected to functional and biochemical pathway analysis using the Gene Ontology (GO), Kyoto Encyclopedia of Genes and Genomes (KEGG), and Reactome pathway databases. Goseq was used to perform the GO enrichment analysis and Kobas was used to perform the pathway analysis.

qPCR analysis

One microgram of total RNA from renal cortical tissues or cultured RTECs was reverse transcribed using RevertAid First Strand cDNA Synthesis Kit (Thermo Fisher Scientific), and qRT-PCR was run in QuantStudio 7 Flex Real-Time PCR System (Thermo Fisher Scientific) using SYBR Green Master Mix and gene-specific primers. The expression levels of the samples were determined by the comparative CT ($\Delta\Delta^{CT}$) method. β-actin was used as the internal control. For gene expression analysis in RTECs *in vivo*, anti-GFP antibody and magnetic-activated cell sorting (MACS) columns (Miltenyi Biotec) were used to isolate GFP-positive tubular epithelial cells from the kidneys of reporter mice with membrane-localized enhanced GFP (EGFP) as reported previously (31).

Immunoblot analysis and ELISA

Whole-cell lysates from renal cortical tissues were prepared using modified RIPA buffer (20 mM Tris-HCl, pH 7.5, 150 mM NaCl, 1 mM Na2EDTA, 1 mM EGTA, 1% Nonidet P-40, 2.5 mM sodium pyrophosphate, 1 mM β-glycerophosphate, protease, and phosphatase inhibitors) supplemented with 1% SDS. Invitrogen Bis-Tris gradient midi-gels were used for Western blotting analysis, followed by detection by ECL reagent (Cell Signaling). Primary antibodies used for Western blotting analysis were from Santa Cruz Biotechnology (Vgf (sc-365397) and β-actin (47778)) and were used at 1:1000 dilution. Secondary antibodies were from Jackson Immunoresearch Laboratories and were used at 1:2000 dilutions. Densitometric analysis was carried out using Image J, and the signals of target protein were normalized to actin levels in the same samples.

For measurement of TLQP-21 secretion in the media, primary murine RTECs were treated with vehicle or 50 μM cisplatin followed by media collection after 12 h. Secreted TLQP-21 was assayed from the media using a mice TLQP-21-specific ELISA (Peninsula Laboratories International, S-1477) and normalized to cellular protein levels (BCA assay, Thermo Fisher Scientific). Similar methodology was used to measure TLQP-21 levels in cellular lysates. *Vgf* knockout samples were used as negative controls in all the experiments, and TLQP-21 levels were undetected in the *Vgf*-deficient cells and tissues.

Immunofluorescence staining

Vgf immunostaining was performed according to methods described previously (64). Briefly, frozen renal tissues were cryosectioned and fixed with 4% paraformaldehyde, followed by permeabilization with 1% Triton X-100. Subsequently, the tissue sections were sequentially incubated with a blocking buffer, the Vgf antibody (Santa Cruz Biotechnology, sc-365397), FITC-labeled anti-mouse secondary antibody (Abcam, ab6785), and mounting with DAPI containing fluoroshield media (Abcam, ab104139). The staining was then examined by fluorescence microscopy. *Vgf* knockout tissues were used as negative controls and did not have any positive Vgf staining.

TLQP-21 add-back experiments

Murine purified TLQP-21 (Sigma-Aldrich, T1581) and a scrambled control peptide (GenScript) were used for add-back experiments. For *in vivo* experiments, littermate control and *Vgf*-deficient male mice (8–12 weeks) were injected with cisplatin (30 mg/kg, intraperitoneal). Twelve hours later, TLQP-21 or control scrambled peptide was administered by intraperitoneal injection (4.5 mg/kg). Renal tissues and blood were collected at 72 h post cisplatin injection, followed by assessment of renal damage. For *in vitro* experiments, primary RTECs were sequentially treated with 50 μM cisplatin (or vehicle), followed by TLQP21 or scrambled peptide (25 nM) treatment four hours later and assessment of cellular viability at 24 or 48 h.

Promoter luciferase assay

HEK293 cells were stably transfected with either empty vector (pCMV6) or Sox9 expression vector (OriGene). These cells were then utilized for promoter luciferase reporter assays using methods reported in our recent studies (31, 65). Briefly, 5×10^3 cells were plated overnight on white poly-L-lysine–coated 96-well plates, followed by transient transfection with either promoter constructs (Switchgear Genomics, encoding ~2 kb sequence upstream of transcription start site of *Vgf*) or empty promoter construct at 30 ng in combination with the Cypridina TK control construct (Switchgear Genomics) at 1 ng, according to the manufacturer's protocol (Switchgear Genomics, Lightswitch Dual Assay kit, DA010). The promoter construct encodes a Renilla luminescent reporter gene, called RenSP, whereas the transfection and normalization vector encodes a Cypridina luciferase. The Renilla luciferase activity was normalized to the Cypridina luciferase activity.

Site-directed mutagenesis

The QuikChange II XL Site-Directed Mutagenesis Kit (Agilent Technologies) was utilized to generate *Vgf* promoter mutants, according to previously described methods (66). The QuikChange primer design program was used to design mutagenesis primers, and primers were synthesized by Integrated DNA Technologies. Mutant constructs were sequenced to confirm successful mutagenesis. The primers used for Sox9 binding-site mutagenesis (ATTGTT to AAACAT) in the murine *Vgf* promoter-reporter construct were 5′-TGTTCCCTGGTCCATGTTTAAGTTCAAGCCGACAGCATCACCCAG-3′ and 5′-CTGGGTGATGCTGTCGGCTTGAACTTAAACATGGACCAGGGAACA-3′ and in the human promoter-reporter construct were 5′-CTTGGTGGTACACATGTTTGTGTGTGTAAGCACACACATGCCCCC-3′ and

5′-GGGGGCATGTGTGTGCTTACACACACAAACATG-TGTACCACCAAG-3′.

ChIP

ChIP assays were performed using the Pierce Magnetic ChIP Kit according to the manufacturer's instructions and our previous studies (31, 65). Briefly, cross-linking with 1% formaldehyde was carried out in renal tissues, followed by quenching with glycine, harvesting, and DNA fragmentation by sonication. Tissue lysates were precleared for 2 h with Protein A + G magnetic beads (EMD Millipore). Precleared lysates were then incubated with 5 μg of anti-Sox9 antibody (Abcam, ab3697) overnight at 4 °C, followed by addition of Protein A + G magnetic beads and incubation for 4 h at 4 °C. Finally, the beads were collected and repeatedly washed, and the protein–DNA complexes were eluted, cross-links were reversed, and the DNA was purified. Standard qPCR analysis was then carried out using the following primers spanning the *Vgf* promoter: 5′-TCCCAGGCTGATGTGAA-CTT-3′ and 5′-TCACCAGGCATGCCCATAAG-3′.

Human kidney organoid cultures and epithelial cell isolation

All work was carried out with the approval of the University of Auckland Human Participants Ethics and Health and Disability Ethics Committees (UAHPEC 8712 and HDEC 17/NTA/204, respectively) and the University of Auckland Biological Safety Committee. Kidney organoids were generated from the MANZ-2 iPSC line, and day-12 organoids were treated with 4 × 5 μM cisplatin over 7 days to induce AKI as described previously (43, 67). On day 19, epithelial cells were isolated using EPCAM MACS as described previously (68). Briefly, organoids were enzymatically dissociated and the cell suspension was then passed sequentially through 100, 40, and 20 μM cell strainers and centrifuged for 10 min at 300 × *g*. The cells were resuspended in 250 μl of MACS buffer plus 50 μl of EPCAM (CD326) microbeads (Miltenyi Biotech) and incubated for 30 min at 4 °C. The cells were washed with MACS buffer and centrifuged twice prior to resuspension in 500 μl of MACS buffer. The cell suspension was then passed through an MS MACS column according to the manufacturer's instruction (Miltenyi Biotec). The flow-through (EPCAM −ve fraction) was collected, and the EPCAM +ve fraction was eluted with 1 ml of MACS buffer from the column. The EPCAM −ve and EPCAM +ve fractions were pelleted by centrifugation at 300 × *g* for 10 min. Total RNA was prepared from EPCAM +ve cells and quantitative PCR was performed with gene-specific primers. Gene expression was determined by the comparative CT ($\Delta\Delta^{CT}$) method using HPRT1 as the internal control. Primer sequences were as follows: HPRT1 (5′-CATTATGCTGAG-GATTTGGAAAGG-3′ and 5′-CTTGAGCACACAGAGGGC-TACA-3′), SOX9 (5′-AGCGAACGCACATCAAGAC-3′ and 5′-CTGTAGGCGATCTGTTGGGG-3′), and VGF (5′-CCT-TCCCGAAACCCACAAGTT-3′ and 5′-GCCTTGGTACGC-CTTGGAC-3′).

Statistical analysis

Data in all the graphs are presented as mean with S.E. unless stated otherwise. Statistical calculations were carried out using GraphPad Prism. $p < 0.05$ was considered statistically significant. To calculate statistical significance between two groups, two-tailed unpaired Student's *t* test was performed. One-way analysis of variance (ANOVA) followed by Tukey's or Dunnett's multiple-comparison test was used for comparisons among three or more groups. No sample outliers were excluded.

Data availability

The RNA-seq data have been deposited in the Gene Expression Omnibus (GSE153625). The rest of data are contained within this article and in the supporting information.

Acknowledgments—We thank Simarjot Pabla and Sithara Raju Ponny (University of Massachusetts) for assistance with RNA-seq data analysis and submission. We also thank Eric Liao and Sophia Wang (Quick Biology, Pasadena, CA) for assistance with transcriptome analysis. We thank Dr. Zheng Dong (Augusta University) for providing the BUMPT cell line, which was originally obtained from Drs. Wilfred Lieberthal and John Schwartz, Boston University School of Medicine, Boston, MA. We thank all members of our laboratories for helpful discussions of this study and critical reading of the manuscript.

Author contributions—J. Y. K. and N. S. P. conceptualization; J. Y. K., L. A. J., T. P., S. V. P., D. S. G., A. J. D., V. S., M.-A. S., A. B., and N. S. P. data curation; J. Y. K., L. A. J., M. G., T. P., S. V. P., A. J. D., V. S., M.-A. S., A. B., and N. S. P. formal analysis; J. Y. K., Y. B., L. A. J., and N. S. P. validation; J. Y. K., L. A. J., F. A., M. G., D. S. G., V. S., and N. S. P. investigation; J. Y. K., L. A. J., and M.-A. S. visualization; J. Y. K., Y. B., L. A. J., F. A., M. G., D. S. G., V. S., M.-A. S., and N. S. P. methodology; J. Y. K. and N. S. P. writing-original draft; J. Y. K., M.-A. S., A. B., and N. S. P. writing-review and editing; A. J. D. and N. S. P. funding acquisition; N. S. P. supervision; N. S. P. project administration.

Funding and additional information—This study was supported by funds from the Ohio State University Comprehensive Cancer Center, National Institutes of Health (NIH) Grant R01DK117183 (to A. B.), American Heart Association Scientist Development Grant 17SDG33440070 (to N. S. P.), and American Heart Association postdoctoral fellowship 18POST33990282 (to Y. B.). Studies in the Davidson laboratory were supported by the Health Research Council of New Zealand (17/425), the National Institute of Diabetes and Digestive and Kidney Diseases (R01-DK-069403), and the United States Army Medical Research and Development Command (W81XWH-17-1-0610). The content is solely the responsibility of the authors and does not necessarily represent the official views of the National Institutes of Health.

Conflict of interest—The authors declare that they have no conflicts of interest with the contents of this article.

Abbreviations—The abbreviations used are: AKI, acute kidney injury; RTEC, renal tubular epithelial cells; Sox9, SRY-box

transcription factor 9; IRI, ischemia-reperfusion injury; GO, gene ontology; BUMPT, Boston University mouse proximal tubule cells; MTT, 3-(4,5-dimethylthiazol-2-yl)-2,5-diphenyltetrazolium bromide; TMM, trimmed mean of M-values; MACS, magnetic-activated cell sorting; EGFP, enhanced GFP; HK-2, human kidney 2.

References

1. Zuk, A., and Bonventre, J. V. (2016) Acute kidney injury. *Annu. Rev. Med.* **67,** 293–307 CrossRef Medline
2. Peerapornratana, S., Manrique-Caballero, C. L., Gómez, H., and Kellum, J. A. (2019) Acute kidney injury from sepsis: current concepts, epidemiology, pathophysiology, prevention and treatment. *Kidney Int.* **96,** 1083–1099 CrossRef Medline
3. Bosch, X., Poch, E., and Grau, J. M. (2009) Rhabdomyolysis and acute kidney injury. *N. Engl. J. Med.* **361,** 62–72 CrossRef Medline
4. Wang, Y., and Bellomo, R. (2017) Cardiac surgery-associated acute kidney injury: risk factors, pathophysiology and treatment. *Nat. Rev. Nephrol.* **13,** 697–711 CrossRef Medline
5. Rosner, M. H., and Perazella, M. A. (2017) Acute kidney injury in patients with cancer. *N. Engl. J. Med.* **376,** 1770–1781 CrossRef Medline
6. Bonventre, J. V., and Yang, L. (2011) Cellular pathophysiology of ischemic acute kidney injury. *J. Clin. Invest.* **121,** 4210–4221 CrossRef Medline
7. Bellomo, R., Kellum, J. A., and Ronco, C. (2012) Acute kidney injury. *Lancet* **380,** 756–766 CrossRef Medline
8. Chawla, L. S., Eggers, P. W., Star, R. A., and Kimmel, P. L. (2014) Acute kidney injury and chronic kidney disease as interconnected syndromes. *N. Engl. J. Med.* **371,** 58–66 CrossRef Medline
9. Linkermann, A., Chen, G., Dong, G., Kunzendorf, U., Krautwald, S., and Dong, Z. (2014) Regulated cell death in AKI. *J. Am. Soc. Nephrol.* **25,** 2689–2701 CrossRef Medline
10. Kaushal, G. P., and Shah, S. V. (2016) Autophagy in acute kidney injury. *Kidney Int.* **89,** 779–791 CrossRef Medline
11. Cummings, B. S., and Schnellmann, R. G. (2002) Cisplatin-induced renal cell apoptosis: caspase 3-dependent and -independent pathways. *J. Pharmacol. Exp. Ther.* **302,** 8–17 CrossRef Medline
12. Arany, I., Megyesi, J. K., Kaneto, H., Price, P. M., and Safirstein, R. L. (2004) Cisplatin-induced cell death is EGFR/src/ERK signaling dependent in mouse proximal tubule cells. *Am. J. Physiol. Renal Physiol* **287,** F543–F549 CrossRef Medline
13. Jankowski, J., Perry, H. M., Medina, C. B., Huang, L., Yao, J., Bajwa, A., Lorenz, U. M., Rosin, D. L., Ravichandran, K. S., Isakson, B. E., and Okusa, M. D. (2018) Epithelial and endothelial pannexin1 channels mediate AKI. *J. Am. Soc. Nephrol.* **29,** 1887–1899 CrossRef Medline
14. Basile, D. P., and Yoder, M. C. (2014) Renal endothelial dysfunction in acute kidney ischemia reperfusion injury. *Cardiovasc. Hematol. Disord. Drug Targets* **14,** 3–14 CrossRef Medline
15. Bullen, A., Liu, Z. Z., Hepokoski, M., Li, Y., and Singh, P. (2017) Renal oxygenation and hemodynamics in kidney injury. *Nephron* **137,** 260–263 CrossRef Medline
16. Ramesh, G., and Reeves, W. B. (2002) TNF-α mediates chemokine and cytokine expression and renal injury in cisplatin nephrotoxicity. *J. Clin. Invest.* **110,** 835–842 CrossRef Medline
17. Bajwa, A., Kinsey, G. R., and Okusa, M. D. (2009) Immune mechanisms and novel pharmacological therapies of acute kidney injury. *Curr. Drug Targets* **10,** 1196–1204 CrossRef Medline
18. Salton, S. R., Ferri, G. L., Hahm, S., Snyder, S. E., Wilson, A. J., Possenti, R., and Levi, A. (2000) VGF: a novel role for this neuronal and neuroendocrine polypeptide in the regulation of energy balance. *Front. Neuroendocrinol.* **21,** 199–219 CrossRef Medline
19. Lewis, J. E., Brameld, J. M., and Jethwa, P. H. (2015) Neuroendocrine role for VGF. *Front. Endocrinol.* **6,** 3 CrossRef Medline
20. Hahm, S., Mizuno, T. M., Wu, T. J., Wisor, J. P., Priest, C. A., Kozak, C. A., Boozer, C. N., Peng, B., McEvoy, R. C., Good, P., Kelley, K. A., Takahashi, J. S., Pintar, J. E., Roberts, J. L., Mobbs, C. V., *et al.* (1999) Targeted deletion of the Vgf gene indicates that the encoded secretory peptide precursor plays a novel role in the regulation of energy balance. *Neuron* **23,** 537–548 CrossRef Medline
21. Hunsberger, J. G., Newton, S. S., Bennett, A. H., Duman, C. H., Russell, D. S., Salton, S. R., and Duman, R. S. (2007) Antidepressant actions of the exercise-regulated gene VGF. *Nat. Med.* **13,** 1476–1482 CrossRef Medline
22. Alder, J., Thakker-Varia, S., Bangasser, D. A., Kuroiwa, M., Plummer, M. R., Shors, T. J., and Black, I. B. (2003) Brain-derived neurotrophic factor-induced gene expression reveals novel actions of VGF in hippocampal synaptic plasticity. *J. Neurosci.* **23,** 10800–10808 CrossRef Medline
23. Stephens, S. B., Edwards, R. J., Sadahiro, M., Lin, W. J., Jiang, C., Salton, S. R., and Newgard, C. B. (2017) The prohormone VGF regulates β cell function via insulin secretory granule biogenesis. *Cell Rep.* **20,** 2480–2489 CrossRef Medline
24. Pabla, N., and Dong, Z. (2008) Cisplatin nephrotoxicity: mechanisms and renoprotective strategies. *Kidney Int.* **73,** 994–1007 CrossRef Medline
25. Ralto, K. M., Rhee, E. P., and Parikh, S. M. (2020) NAD(+) homeostasis in renal health and disease. *Nat. Rev. Nephrol.* **16,** 99–111 CrossRef Medline
26. Kang, H. M., Ahn, S. H., Choi, P., Ko, Y. A., Han, S. H., Chinga, F., Park, A. S., Tao, J., Sharma, K., Pullman, J., Bottinger, E. P., Goldberg, I. J., and Susztak, K. (2015) Defective fatty acid oxidation in renal tubular epithelial cells has a key role in kidney fibrosis development. *Nat. Med.* **21,** 37–46 CrossRef Medline
27. Ichimura, T., Bonventre, J. V., Bailly, V., Wei, H., Hession, C. A., Cate, R. L., and Sanicola, M. (1998) Kidney injury molecule-1 (KIM-1), a putative epithelial cell adhesion molecule containing a novel immunoglobulin domain, is up-regulated in renal cells after injury. *J. Biol. Chem.* **273,** 4135–4142 CrossRef Medline
28. Paragas, N., Qiu, A., Zhang, Q., Samstein, B., Deng, S. X., Schmidt-Ott, K. M., Viltard, M., Yu, W., Forster, C. S., Gong, G., Liu, Y., Kulkarni, R., Mori, K., Kalandadze, A., Ratner, A. J., *et al.* (2011) The Ngal reporter mouse detects the response of the kidney to injury in real time. *Nat. Med.* **17,** 216–222 CrossRef Medline
29. Takeuchi, H., Inagaki, S., Morozumi, W., Nakano, Y., Inoue, Y., Kuse, Y., Mizoguchi, T., Nakamura, S., Funato, M., Kaneko, H., Hara, H., and Shimazawa, M. (2018) VGF nerve growth factor inducible is involved in retinal ganglion cells death induced by optic nerve crush. *Sci. Rep.* **8,** 16443 CrossRef Medline
30. Shimazawa, M., Tanaka, H., Ito, Y., Morimoto, N., Tsuruma, K., Kadokura, M., Tamura, S., Inoue, T., Yamada, M., Takahashi, H., Warita, H., Aoki, M., and Hara, H. (2010) An inducer of VGF protects cells against ER stress-induced cell death and prolongs survival in the mutant SOD1 animal models of familial ALS. *PLoS ONE* **5,** e15307 CrossRef Medline
31. Kim, J. Y., Bai, Y., Jayne, L. A., Hector, R. D., Persaud, A. K., Ong, S. S., Rojesh, S., Raj, R., Feng, M., Chung, S., Cianciolo, R. E., Christman, J. W., Campbell, M. J., Gardner, D. S., Baker, S. D., *et al.* (2020) A kinome-wide screen identifies a CDKL5-SOX9 regulatory axis in epithelial cell death and kidney injury. *Nat. Commun.* **11,** 1924 CrossRef Medline
32. Iwano, M., Plieth, D., Danoff, T. M., Xue, C., Okada, H., and Neilson, E. G. (2002) Evidence that fibroblasts derive from epithelium during tissue fibrosis. *J. Clin. Invest.* **110,** 341–350 CrossRef Medline
33. Severini, C., Ciotti, M. T., Biondini, L., Quaresima, S., Rinaldi, A. M., Levi, A., Frank, C., and Possenti, R. (2008) TLQP-21, a neuroendocrine VGF-derived peptide, prevents cerebellar granule cells death induced by serum and potassium deprivation. *J. Neurochem.* **104,** 534–544 CrossRef Medline
34. Stephens, S. B., Schisler, J. C., Hohmeier, H. E., An, J., Sun, A. Y., Pitt, G. S., and Newgard, C. B. (2012) A VGF-derived peptide attenuates development of type 2 diabetes via enhancement of islet β-cell survival and function. *Cell Metab.* **16,** 33–43 CrossRef Medline
35. Hannedouche, S., Beck, V., Leighton-Davies, J., Beibel, M., Roma, G., Oakeley, E. J., Lannoy, V., Bernard, J., Hamon, J., Barbieri, S., Preuss, I., Lasbennes, M. C., Sailer, A. W., Suply, T., Seuwen, K., *et al.* (2013) Identification of the C3a receptor (C3AR1) as the target of the VGF-derived peptide TLQP-21 in rodent cells. *J. Biol. Chem.* **288,** 27434–27443 CrossRef Medline
36. Chen, Y. C., Pristerá, A., Ayub, M., Swanwick, R. S., Karu, K., Hamada, Y., Rice, A. S., and Okuse, K. (2013) Identification of a receptor for neuropeptide VGF and its role in neuropathic pain. *J. Biol. Chem.* **288,** 34638–34646 CrossRef Medline

37. Guo, Z., Sahu, B. S., He, R., Finan, B., Cero, C., Verardi, R., Razzoli, M., Veglia, G., Di Marchi, R. D., Miles, J. M., and Bartolomucci, A. (2018) Clearance kinetics of the VGF-derived neuropeptide TLQP-21. *Neuropeptides* **71,** 97–103 CrossRef Medline
38. Kumar, S., Liu, J., Pang, P., Krautzberger, A. M., Reginensi, A., Akiyama, H., Schedl, A., Humphreys, B. D., and McMahon, A. P. (2015) Sox9 activation highlights a cellular pathway of renal repair in the acutely injured mammalian kidney. *Cell Rep.* **12,** 1325–1338 CrossRef Medline
39. Liu, J., Kumar, S., Dolzhenko, E., Alvarado, G. F., Guo, J., Lu, C., Chen, Y., Li, M., Dessing, M. C., Parvez, R. K., Cippà, P. E., Krautzberger, A. M., Saribekyan, G., Smith, A. D., and McMahon, A. P. (2017) Molecular characterization of the transition from acute to chronic kidney injury following ischemia/reperfusion. *JCI Insight* **2,** CrossRef Medline
40. Kang, H. M., Huang, S., Reidy, K., Han, S. H., Chinga, F., and Susztak, K. (2016) Sox9-positive progenitor cells play a key role in renal tubule epithelial regeneration in mice. *Cell Rep.* **14,** 861–871 CrossRef Medline
41. Kumar, S. (2018) Cellular and molecular pathways of renal repair after acute kidney injury. *Kidney Int.* **93,** 27–40 CrossRef Medline
42. Gardner, D. S., De Brot, S., Dunford, L. J., Grau-Roma, L., Welham, S. J., Fallman, R., O'Sullivan, S. E., Oh, W., and Devonald, M. A. (2016) Remote effects of acute kidney injury in a porcine model. *Am. J. Physiol. Renal Physiol.* **310,** F259–F271 CrossRef Medline
43. Digby, J. L. M., Vanichapol, T., Przepiorski, A., Davidson, A. J., and Sander, V. (2020) Evaluation of cisplatin-induced injury in human kidney organoids. *Am. J. Physiol. Renal Physiol.* **318,** F971–F978 CrossRef Medline
44. Kishi, S., Brooks, C. R., Taguchi, K., Ichimura, T., Mori, Y., Akinfolarin, A., Gupta, N., Galichon, P., Elias, B. C., Suzuki, T., Wang, Q., Gewin, L., Morizane, R., and Bonventre, J. V. (2019) Proximal tubule ATR regulates DNA repair to prevent maladaptive renal injury responses. *J. Clin. Invest.* **129,** 4797–4816 CrossRef Medline
45. Chang-Panesso, M., Kadyrov, F. F., Lalli, M., Wu, H., Ikeda, S., Kefaloyianni, E., Abdelmageed, M. M., Herrlich, A., Kobayashi, A., and Humphreys, B. D. (2019) FOXM1 drives proximal tubule proliferation during repair from acute ischemic kidney injury. *J. Clin. Invest.* **129,** 5501–5517 CrossRef Medline
46. Thakker-Varia, S., and Alder, J. (2009) Neuropeptides in depression: role of VGF. *Behav. Brain Res.* **197,** 262–278 CrossRef Medline
47. Fairbanks, C. A., Peterson, C. D., Speltz, R. H., Riedl, M. S., Kitto, K. F., Dykstra, J. A., Braun, P. D., Sadahiro, M., Salton, S. R., and Vulchanova, L. (2014) The VGF-derived peptide TLQP-21 contributes to inflammatory and nerve injury-induced hypersensitivity. *Pain* **155,** 1229–1237 CrossRef Medline
48. Hohmeier, H. E., Zhang, L., Taylor, B., Stephens, S., Lu, D., McNamara, P., Laffitte, B., and Newgard, C. B. (2020) Identification of a small molecule that stimulates human β-cell proliferation and insulin secretion, and protects against cytotoxic stress in rat insulinoma cells. *PLoS ONE* **15,** e0224344 CrossRef Medline
49. Bartolomucci, A., Possenti, R., Levi, A., Pavone, F., and Moles, A. (2007) The role of the vgf gene and VGF-derived peptides in nutrition and metabolism. *Genes Nutr.* **2,** 169–180 CrossRef Medline
50. Cero, C., Vostrikov, V. V., Verardi, R., Severini, C., Gopinath, T., Braun, P. D., Sassano, M. F., Gurney, A., Roth, B. L., Vulchanova, L., Possenti, R., Veglia, G., and Bartolomucci, A. (2014) The TLQP-21 peptide activates the G-protein-coupled receptor C3aR1 via a folding-upon-binding mechanism. *Structure* **22,** 1744–1753 CrossRef Medline
51. Sahu, B. S., Rodriguez, P., Nguyen, M. E., Han, R., Cero, C., Razzoli, M., Piaggi, P., Laskowski, L. J., Pavlicev, M., Muglia, L., Mahata, S. K., O'Grady, S., McCorvy, J. D., Baier, L. J., Sham, Y. Y., *et al.* (2019) Peptide/receptor co-evolution explains the lipolytic function of the neuropeptide TLQP-21. *Cell Rep.* **28,** 2567–2580.e6 CrossRef Medline
52. El Gaamouch, F., Audrain, M., Lin, W. J., Beckmann, N., Jiang, C., Hariharan, S., Heeger, P. S., Schadt, E. E., Gandy, S., Ehrlich, M. E., and Salton, S. R. (2020) VGF-derived peptide TLQP-21 modulates microglial function through C3aR1 signaling pathways and reduces neuropathology in 5xFAD mice. *Mol. Neurodegener.* **15,** 4 CrossRef Medline
53. Cero, C., Razzoli, M., Han, R., Sahu, B. S., Patricelli, J., Guo, Z., Zaidman, N. A., Miles, J. M., O'Grady, S. M., and Bartolomucci, A. (2017) The neuropeptide TLQP-21 opposes obesity via C3aR1-mediated enhancement of adrenergic-induced lipolysis. *Mol. Metab.* **6,** 148–158 CrossRef Medline
54. Peng, Q., Li, K., Smyth, L. A., Xing, G., Wang, N., Meader, L., Lu, B., Sacks, S. H., and Zhou, W. (2012) C3a and C5a promote renal ischemia-reperfusion injury. *J. Am. Soc. Nephrol.* **23,** 1474–1485 CrossRef Medline
55. Sharfuddin, A. A., and Molitoris, B. A. (2011) Pathophysiology of ischemic acute kidney injury. *Nat. Rev. Nephrol.* **7,** 189–200 CrossRef Medline
56. Jang, H. R., and Rabb, H. (2009) The innate immune response in ischemic acute kidney injury. *Clin. Immunol.* **130,** 41–50 CrossRef Medline
57. Rabb, H., Griffin, M. D., McKay, D. B., Swaminathan, S., Pickkers, P., Rosner, M. H., Kellum, J. A., Ronco, C., and Acute Dialysis Quality Initiative Consensus, X. W. G, Acute Dialysis Quality Initiative Consensus XIII Work Group, (2016) Inflammation in AKI: current understanding, key questions, and knowledge gaps. *J. Am. Soc. Nephrol.* **27,** 371–379 CrossRef Medline
58. Inoue, T., Tanaka, S., and Okusa, M. D. (2017) Neuroimmune interactions in inflammation and acute kidney injury. *Front. Immunol.* **8,** 945 CrossRef Medline
59. Bajwa, A., Jo, S. K., Ye, H., Huang, L., Dondeti, K. R., Rosin, D. L., Haase, V. H., Macdonald, T. L., Lynch, K. R., and Okusa, M. D. (2010) Activation of sphingosine-1-phosphate 1 receptor in the proximal tubule protects against ischemia-reperfusion injury. *J. Am. Soc. Nephrol.* **21,** 955–965 CrossRef Medline
60. Soliman, N., Okuse, K., and Rice, A. S. C. (2019) VGF: a biomarker and potential target for the treatment of neuropathic pain? *Pain Rep.* **4,** e786 CrossRef Medline
61. Pabla, N., Dong, G., Jiang, M., Huang, S., Kumar, M. V., Messing, R. O., and Dong, Z. (2011) Inhibition of PKCδ reduces cisplatin-induced nephrotoxicity without blocking chemotherapeutic efficacy in mouse models of cancer. *J. Clin. Invest.* **121,** 2709–2722 CrossRef Medline
62. Kim, J. Y., Jayne, L. A., Bai, Y., Feng, M. J. H. H., Clark, M. A., Chung, S., W Christman, J., Cianciolo, R. E., and Pabla, N. S. (2020) Ribociclib mitigates cisplatin-associated kidney injury through retinoblastoma-1 dependent mechanisms. *Biochem. Pharmacol.* **177,** 113939 CrossRef Medline
63. Pabla, N., Gibson, A. A., Buege, M., Ong, S. S., Li, L., Hu, S., Du, G., Sprowl, J. A., Vasilyeva, A., Janke, L. J., Schlatter, E., Chen, T., Ciarimboli, G., and Sparreboom, A. (2015) Mitigation of acute kidney injury by cell-cycle inhibitors that suppress both CDK4/6 and OCT2 functions. *Proc. Natl. Acad. Sci. U. S. A.* **112,** 5231–5236 CrossRef Medline
64. Pabla, N., Murphy, R. F., Liu, K., and Dong, Z. (2009) The copper transporter Ctr1 contributes to cisplatin uptake by renal tubular cells during cisplatin nephrotoxicity. *Am. J. Physiol. Renal Physiol.* **296,** F505–F511 CrossRef Medline
65. van Oosterwijk, J. G., Buelow, D. R., Drenberg, C. D., Vasilyeva, A., Li, L., Shi, L., Wang, Y. D., Finkelstein, D., Shurtleff, S. A., Janke, L. J., Pounds, S., Rubnitz, J. E., Inaba, H., Pabla, N., and Baker, S. D. (2018) Hypoxia-induced upregulation of BMX kinase mediates therapeutic resistance in acute myeloid leukemia. *J. Clin. Invest.* **128,** 369–380 CrossRef Medline
66. Sprowl, J. A., Ong, S. S., Gibson, A. A., Hu, S., Du, G., Lin, W., Li, L., Bharill, S., Ness, R. A., Stecula, A., Offer, S. M., Diasio, R. B., Nies, A. T., Schwab, M., Cavaletti, G., *et al.* (2016) A phosphotyrosine switch regulates organic cation transporters. *Nat. Commun.* **7,** 10880 CrossRef Medline
67. Przepiorski, A., Sander, V., Tran, T., Hollywood, J. A., Sorrenson, B., Shih, J. H., Wolvetang, E. J., McMahon, A. P., Holm, T. M., and Davidson, A. J. (2018) A simple bioreactor-based method to generate kidney organoids from pluripotent stem cells. *Stem Cell Reports* **11,** 470–484 CrossRef Medline
68. Forbes, T. A., Howden, S. E., Lawlor, K., Phipson, B., Maksimovic, J., Hale, L., Wilson, S., Quinlan, C., Ho, G., Holman, K., Bennetts, B., Crawford, J., Trnka, P., Oshlack, A., Patel, C., *et al.* (2018) Patient-iPSC-derived kidney organoids show functional validation of a ciliopathic renal phenotype and reveal underlying pathogenetic mechanisms. *Am. J. Hum. Genet.* **102,** 816–831 CrossRef Medline